Bosonic analogs of the fractional quantum Hall state in the vicinity of Mott states

Yoshihito Kuno, Keita Shimizu, and Ikuo Ichinose
Department of Applied Physics, Nagoya Institute of Technology, Nagoya, 466-8555 Japan
(Received 5 October 2016; published 6 January 2017)

In this paper, the Bose-Hubbard model (BHM) with the nearest-neighbor (NN) repulsions is studied from the viewpoint of possible bosonic analogs of the fractional quantum Hall (FQH) state in the vicinity of the Mott insulator (MI). First, by means of the Gutzwiller approximation, we obtain the phase diagram of the BHM in a magnetic field. Then, we introduce an effective Hamiltonian describing excess particles on a MI and calculate the vortex density, momentum distribution, and the energy gap. These calculations indicate that the vortex solid forms for small NN repulsions, but a homogeneous featureless "Bose metal" takes the place of it as the NN repulsion increases. We consider particular filling factors at which the bosonic FQH state is expected to form. Chern-Simons (CS) gauge theory to the excess particle is introduced, and a modified Gutzwiller wave function, which describes bosons with attached flux quanta, is introduced. The energy of the excess particles in the bosonic FQH state is calculated using that wave function, and it is compared with the energy of the vortex solid and Bose metal. We found that the energy of the bosonic FQH state is lower than that of the Bose metal and comparable with the vortex solid. Finally, we clarify the condition that the composite fermion appears by using CS theory on the lattice that we previously proposed for studying the electron FQH effect.

DOI: 10.1103/PhysRevA.95.013607

I. INTRODUCTION

At present, cold atomic physics in an optical lattice is one of the most intensively studied research fields [1]. This field opened the door for quantum simulation of various important condensed-matter systems, which have been studied for a long time. In particular by the simulation using atomic gases on an optical lattice, we can obtain new knowledge and viewpoint concerning the strongly correlated many-body systems for which the conventional methods cannot clarify the phase diagram, etc. [2]. Recently, synthetic gauge fields mimicking uniform magnetic fields have been created in optical lattice systems by using laser-assisted tunneling in a tilted optical potential [3,4]. The theoretical proposal for this setup was given by Jaksch and Zoller [5]. The experiments can produce much stronger magnetic fields than those obtained by rotating optical lattice systems [6,7]. As a result, it is expected that a system similar to the two-dimensional (2D) electron systems in a strong magnetic field can be produced in the atomic gas system.

In this paper, we focus on Bose-gas systems on a 2D lattice that are analogs of the 2D electron systems subject to a strong magnetic field [8,9]. That is, we study the Bose-Hubbard model (BHM) in a strong synthetic gauge field. In particular, we investigate the possibility of the existence of fractional quantum Hall (FQH) state analogs in this model. In parallel to the experimental progress, there appeared many theoretical studies on the existence of integer quantum Hall and FQH states in boson systems on the lattice [10–15]. In Refs. [11,12,16], the appearance of the FQH-like states was suggested by calculating the overlap of the Laughlin wave function describing the FQH state and a ground-state wave function obtained by the exact diagonalization. Also, applying the composite fermion (CF) theory for the hard-core boson system, some analogous incompressible states to the FQH state on a lattice were studied [13].

In Ref. [17], Umucalilar and Oktel gave an interesting observation that in the regime close to a Mott insulator (MI), excess particles on the Mott state form a FQH analog state at particular filling factors of the excess particle, i.e., the coexistence phase of the Mott state and the hard-core bosonic FQH state may exist. Motivated by this idea, numerical studies [16,18] exhibited the possibility of the existence of FQH analog states in the vicinity of the MI. However, until now, there has been no unified view of the true ground state in the vicinity of the MI in the BHM subject to a strong synthetic magnetic field. Also, the effect of interactions has not been completely understood yet, e.g., how the long-range interactions, like the dipole-dipole interactions, change the ground-state properties. In the optical lattice system, these interactions, as well as the onsite interactions, are highly controllable by selecting a kind of dipolar atoms [19].

In this paper, we shall study the BHM in a strong magnetic field with and without the nearest-neighbor (NN) interactions. In particular, we investigate properties of the ground-states in the vicinity of the MI and effects of the NN interaction on them by using both the Chern-Simons (CS) theory [8,9,20] and a numerical Gutzwiller method [21,22]. For commensurate magnetic fields and particle fillings, the Gutzwiller method shows that a vortex solid forms for weak NN repulsions, whereas for relatively strong NN repulsions, a featureless homogeneous state (we call Bose metal) takes the place of the vortex solid. To investigate the possibility of the bosonic FQH state, we develop the method that we call CS-Gutzwiller wave function. In that wave function, an integer number of flux quanta are attached to each (excess) particle as described by the CS theory. The energy of the states described by the CS-Gutzwiller wave function is compared with that of the vortex solid and Bose metal, and we obtain interesting results.

This paper is organized as follows. In Sec. II, we outline the target BHM and introduce an effective Hamiltonian that describes the excess particle in the vicinity of Mott states. In Sec. III, we carry out the Gutzwiller numerical method for the BHM in a synthetic gauge field, and observe the ground states, vortex configurations, momentum distributions, and an excitation gap on the ground state. Next, we apply the lattice

 ©2017 American Physical Society

CS theory to the BHM and analyze an excitation spectrum and gap by using the Bogoliubov theory in Sec. IV. In Sec. V, we construct the CS-Gutzwiller numerical method and apply it to the excess particle Hamiltonian. Then, we estimate the energy of the CS-Gutzwiller ground states and compare it to the energy of the vortex solid and Bose metal obtained in Sec. III. In Sec. VI, from the view of the CF theory, we discuss the excess particle system and show the condition that the CF picture appears as low-energy excitations. There, the gauge-theoretical consideration plays an important role. Finally, in Sec. VII, we propose an experimental method to detect a ground-state excitation gap for the FQH analog state, and conclude this study. In the Appendix, we consider the practical cold atomic systems and estimate the onsite and NN repulsions. There, the NN repulsion between atoms is provided by the dipole-dipole interaction of atoms.

II. MODEL AND EFFECTIVE HAMILTONIAN IN THE VICINITY OF MOTT PLATEAUS

In this paper, we consider 2D bosonic gases described by the BHM in a strong magnetic field with NN repulsions. The Hamiltonian $H_{\rm BHM}$ of the BHM on the 2D square lattice is given as

$$H_{\rm BHM} = -J\sum_{\langle i,j\rangle}(a_i^\dagger a_j e^{iA_{ij}} + {\rm H.c.}) + \sum_i \frac{U}{2} n_i(n_i-1) + V\sum_{\langle i,j\rangle} n_i n_j - \mu\sum_i n_i, \tag{2.1}$$

where a_i ($a_i^\dagger$) is the boson annihilation (creation) operator at site i and $n_i = a_i^\dagger a_i$. $\langle i,j\rangle$ denotes a pair of NN sites. The parameter J is the NN hopping amplitude, U and V are the onsite and NN repulsions, respectively. In real experiments, a ratio V/U is highly controllable and can be a fairly large value to a certain extent (see the discussion in the Appendix). In this paper, we take the value of V/U up to ~ 0.3. The vector potential A_{ij} represents a uniform magnetic field and satisfies $\sum_{\rm plaquette} A_{ij} = 2\pi f$ with a parameter $0 \leqslant f \leqslant 1$. In this paper, we mostly focus on the case $f = \frac{1}{2}$ and sometimes $f = \frac{1}{3}$, although a generalization to the case $f = t/s$ (s and t coprime integers) is rather straightforward.

As is well known, the BHM has the MI and superfluid (SF) phases, whose phase boundary forms lobes. Figure 1 shows the phase diagram obtained by our Gutzwiller numerical method that we shall explain in a later section. In general, the MI phase is enhanced by the magnetic field, i.e., the lobes elongate compared to the case without the magnetic field. The phase diagram in Fig. 1 is in good agreement with the previous works in Refs. [15–17]. In what follows, we shall study the BHM in the vicinity of the MI of the integer particle filling.

To this end, we consider an effective Hamiltonian that describes particles in the vicinity of the Mott lobes. In Ref. [17], it was discussed that in the regime of a uniform filling $\rho = n + \rho_{\rm ep}$ ($n =$ a positive integer, $0 < \rho_{\rm ep} \ll 1$) the total boson system is divided into two parts: MI part of the filling factor n and the excess particle part of particle density $\rho_{\rm ep}$. In this picture, the excess particles are moving on the solidlike MI. However, as the MI particle and the excess particle are

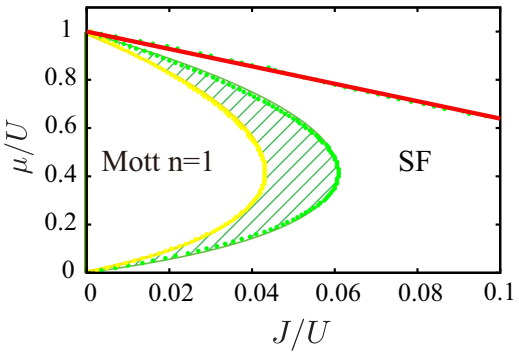

FIG. 1. Obtained phase diagram of the BHM subject to a strong magnetic field. The yellow line is the phase boundary separating the MI and SF states for vanishing magnetic field $f = 0$ obtained by the Gutzwiller numerical method. The green line is an elongated phase boundary as a result of the applied magnetic flux per plaquette, $2\pi f = \pi$. The red line represents the states with the average particle density $\rho = 1.25$.

the same kind of particles, the quantum symmetrization of the Bose particle has to be imposed on the many-particle quantum state.

In the excess particle sector, the hopping parameter of the excess particle changes as $J \to J(n+1)$, and the onsite interaction $U/2 \to U$ from the original ones [15,23], whereas V is intact. Then, the effective Hamiltonian of the excess particle $H_{\rm eBHM}$ is given as

$$H_{\rm eBHM} = -J(n+1)\sum_{\langle i,j\rangle}(c_i^\dagger c_j e^{iA_{ij}} + {\rm H.c.}) + \sum_i U n_{ci}(n_{ci}-1) + V\sum_{\langle i,j\rangle} n_{ci} n_{cj} - \tilde{\mu}\sum_i n_{ci}, \tag{2.2}$$

where c_i ($c_i^\dagger$) is an annihilation (creation) operator of excess boson on site i, the number operator $n_{ci} = c_i^\dagger c_i$, and parameter $\tilde{\mu}$ is the chemical potential for the excess particle.

The above results are derived by the following consideration. The MI state with the filling n is given as

$$|{\rm MI}\rangle = \prod_{i=1}^{N} (a_i^\dagger)^n |0\rangle, \tag{2.3}$$

where N is the total number of lattice sites, and $|0\rangle$ is the vacuum state, which includes no particle. The state $|{\rm MI}\rangle$ is a base state on considering the excess particle Hamiltonian, i.e., its plays a role of the vacuum state of $H_{\rm eBHM}$. Next, we consider one-particle creation on the state $|{\rm MI}\rangle$

$$|1{\rm particle}\rangle \equiv \left(\sum_i \Psi_i^{(k)} a_i^\dagger\right)|{\rm MI}\rangle, \tag{2.4}$$

where $\Psi_i^{(k)}$ is a wave function of the particle. Then, let us consider the hopping energy of this state $|1{\rm particle}\rangle$. To simplify the discussion, we consider a single-particle wave function in the Hofstadter butterfly [24] for $\Psi_i^{(k)}$ with energy $\epsilon_k(f)$. Please notice that $\{\Psi^{(k)}\}$ form a complete set of the Hilbert space of the state vectors. Then, applying the original

hopping term to the state $|1\text{particle}\rangle$, we have

$$\left(\sum_{l,j} t_{lj} a_l^\dagger a_j\right)|1\text{particle}\rangle \to J\epsilon_k(f)(n+1)\left(\sum_i \Psi_i^{(k)} a_i^\dagger\right)|\text{MI}\rangle = J\epsilon_k(f)(n+1)|1\text{particle}\rangle, \quad (2.5)$$

where t_{lj} stands for general hopping amplitudes and $t_{lj} = Je^{iA_{lj}}$ in the present case. From Eq. (2.5), we can see that the hopping energy of the excess particle is given by $(n+1)t_{ij}$. This result is in agreement with the previous results by analytical calculations of the excitation spectrum [23,25] and the numerical study [17]. In intuitive picture, the above result can be understood as follows. There are $(n+1)$ bosons and they are all equal footing and any of them can hop to a NN site, then the hopping amplitude of the excess particle is $(n+1)$-fold of the original one.

Next, we consider the onsite interaction energy for the excess particle. To begin with, we consider one-particle onsite energy deviation from the MI state. To this end, we put $\Psi_i^{(k)} = \delta_{ij}$, which is another complete set of the wave functions. It is rather straightforward to calculate

$$\langle 1\text{particle}|\frac{U}{2}\hat{n}^2|1\text{particle}\rangle - \langle \text{MI}|\frac{U}{2}\hat{n}^2|\text{MI}\rangle = \frac{U}{2}(2n+1). \quad (2.6)$$

Thus, the onsite energy of the state $|1\text{particle}\rangle$ is $\frac{U}{2}(2n+1)$. Similarly, we can consider two-particle onsite energy deviation from the MI state:

$$|2\text{particle}\rangle \equiv (a_j^\dagger)|1\text{particle}\rangle,$$
$$\langle 2\text{particle}|\frac{U}{2}\hat{n}^2|2\text{particle}\rangle - \langle \text{MI}|\frac{U}{2}\hat{n}^2|\text{MI}\rangle = U(2n+2). \quad (2.7)$$

From the above results, the two-body interaction energy of the excess particle is obtained as

$$U(2n+2) - 2\frac{U}{2}(2n+1) = U.$$

Similar discussion on the NN repulsion $V\sum_{\langle i,j\rangle} n_i n_j$ shows that the NN repulsion of the excess particle remains the same. In this way, the effective Hamiltonian H_{eBHM} in Eq. (2.2) is derived.

In the rest of this paper, we shall study the model H_{eBHM} in Eq. (2.2) by means of the numerical as well as analytical methods.

III. NUMERICAL STUDY BY GUTZWILLER APPROXIMATION

In this section, we introduce the Gutzwiller approximation [21,22] that is useful for studying equilibrium states in the strong interaction regime like the MI and its vicinity. Then, in this section by means of the Gutzwiller approximation, we study the system of the total particles described by the Hamiltonian H_{BHM} in Eq. (2.1). In the practical calculation, we mostly focus on the case $f = \frac{1}{2}$ and $n = 1$, and the density of excess particle per site $\rho_{\text{ep}} = \frac{1}{4}$, i.e., the filling fraction of excess particle $\nu_{\text{ep}} = \frac{\rho_{\text{ep}}}{f} = \frac{1}{2}$, i.e., total mean density $\rho = 1.25$.

A. Gutzwiller method

We first introduce a Gutzwiller wave function constructed from the particle number bases of each site i,

$$|\Psi_{\text{GW}}\rangle = \prod_{i=1}^{N}\left(\sum_{n=0}^{n_c} f_n^i |n\rangle_i\right), \quad (3.1)$$

where N is the number of the lattice sites, n_c is a maximum particle number at each site that is a parameter in the Gutzwiller approximation, and the coefficients $\{f_n^i\}$ are variational parameters, which are to be determined by solving the decoupled Hamiltonian given below. As the variational parameters $\{f_n^i\}$ are defined on each site, the total number of parameters is N^{n_c}.

In order to obtain $\{f_n^i\}$ for the ground-state wave function, we employ a mean-field-type approximation, i.e., we decouple the hopping and the NN repulsion terms in H_{BHM} in Eq. (2.1) and derive a single-site Hamiltonian $h_{\text{BHM}i}$. Then, we introduce an order parameter of the SF, i.e., Bose-Einstein condensation (BEC),

$$\Psi_i \equiv \sum_{n_d=1}^{n_c} \sqrt{n_d} f_{n_d-1}^{*i} f_{n_d}^i. \quad (3.2)$$

From Eq. (3.1), it is obvious that $\langle\Psi_{\text{GW}}|a_i|\Psi_{\text{GW}}\rangle = \Psi_i$. With Ψ_i, the local Hamiltonian is given as

$$h_{\text{BHM}i} = -J\sum_{j\in i\text{NN}}(a_i^\dagger e^{iA_{ij}}\Psi_j + \text{H.c.}) + \frac{U}{2}n_i(n_i-1) + Vn_i\left(\sum_{j\in i\text{NN}} n_j\right) - \mu n_i, \quad (3.3)$$

where $j \in i\text{NN}$ denotes the NN sites of site i. From the local Hamiltonian $h_{\text{BHM}i}$, the site energy E_i is estimated as follows by using the wave function $|\Psi_{\text{GW}}\rangle$:

$$\begin{aligned} E_i &= \langle\Psi_{\text{GW}}|h_{\text{BHM}i}|\Psi_{\text{GW}}\rangle \\ &= \sum_{n_d=0}^{n_c}\Bigg\{-J\sum_j\left(\sqrt{n_d} f_{n_d-1}^i e^{iA_{ij}}\Psi_j + \sqrt{n_d+1} f_{n_d+1}^i e^{-iA_{ij}}\Psi_j^*\right) f_{n_d}^{*i} \\ &\quad + \left[\frac{U}{2}n_d(n_d-1) - \mu n_d\right] f_{n_d}^i f_{n_d}^{*i} \\ &\quad + Vn_d f_{n_d}^i f_{n_d}^{*i}\left(\sum_{j\in i\text{NN}}\langle n_j\rangle\right)\Bigg\}, \end{aligned} \quad (3.4)$$

where $\langle n_j\rangle$ is the expectation value of n_j. This local mean-field energy E_i and the mean field Ψ_i form a self-consistent equation. By using an iterative process [15,26], the total energy $E = \sum_i E_i$ can be minimized and both the corresponding variational parameters $f_{n_d}^i$ and order parameter Ψ_i are obtained simultaneously. In our practical calculation, we mostly fix the truncated particle number $n_c = 7$ as this value is expected to be large enough to capture physics in our target regime. We have verified this expectation by varying the value of n_c for some specific quantities. Also, most of the calculations were performed for the linear system size $L = 12$ with the periodic boundary condition.

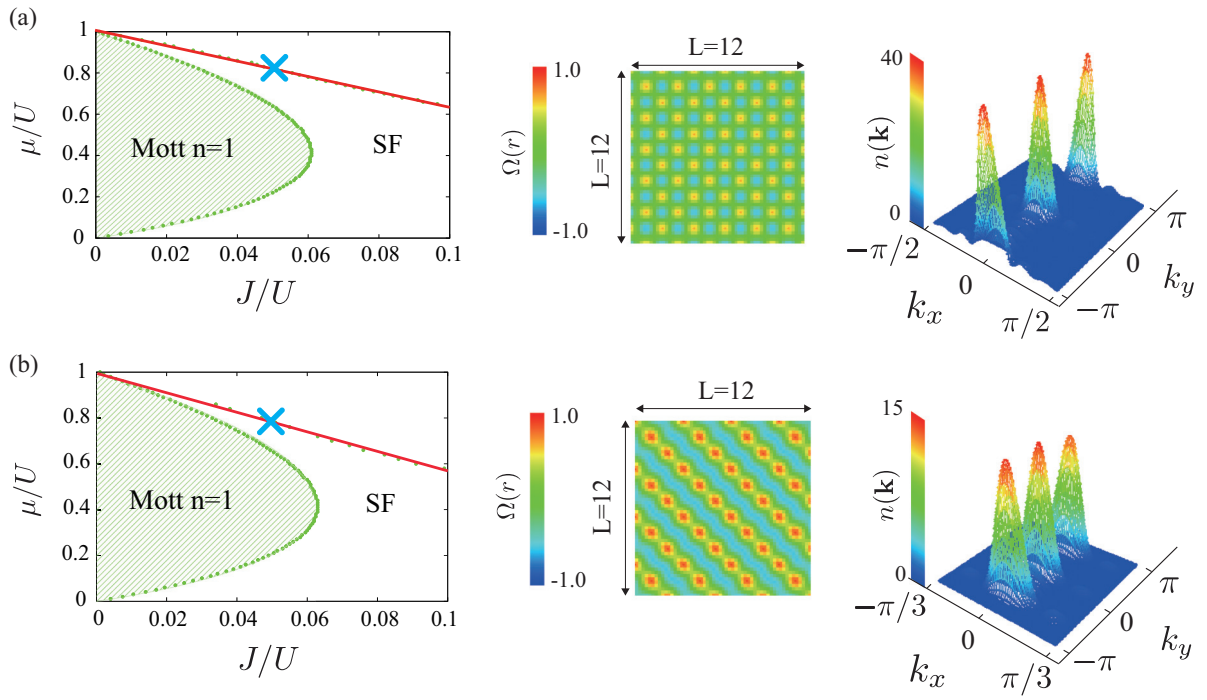

FIG. 2. Numerical results for the $V/U = 0$ and $J/U = 0.05$ cases. The upper panels (a) correspond to the $f = \frac{1}{2}$ case. The phase diagram in the leftmost panel exhibits the point of $\nu_{\rm ep} = \frac{1}{2}$ by the cross $\times$ at which the measurements of vortex density $\Omega(r)$ and the momentum distribution $n(\mathbf{k})$ were performed. The middle and right panels show the calculations of $\Omega(r)$ and $n(\mathbf{k})$, respectively. The lower panels (b) correspond to the $f = \frac{1}{3}$ case ($\nu_{\rm ep} = \frac{1}{2}$). In both cases, the results obviously show that the stable vortex solid forms.

B. Numerical results in the vicinity of the Mott plateaus

In solving the Gutzwiller wave equations practically, there is a point that has to be taken into account carefully. Solution to the Gutzwiller wave equation usually depends on an initial condition [27]. That is, solution sometimes goes to local minimum and does not reach the true ground state due to a large number of the variational parameters $\{f^i_{n_d}\}$. To overcome this difficulty, we performed the calculations by varying the initial configurations in various ways, and searched solutions of the lowest-energy state by trial and error.

To study the ground-state physical properties, we calculated vortex configurations, the density momentum distribution, and also the energy gaps. Vorticity $\Omega(r)$ at the dual lattice site r is given as

$$\Omega(r) = \frac{1}{2\pi}\sum_{\mu,\nu}\epsilon_{\mu\nu}\nabla_\mu J_{i,\nu}, \quad \epsilon_{12} = -\epsilon_{21} = 1,$$
$$\epsilon_{11} = \epsilon_{22} = 0, \quad \nabla_\mu J_{i,\nu} = J_{i+\mu,\nu} - J_{i,\nu}, \tag{3.5}$$

where $J_{i,\nu}$ is a current of Ψ_i in the ν direction defined by the hopping term in the BHM, and explicitly given as $j_{i,\nu} = \frac{1}{4}\sin(\theta_{i+\nu} - \theta_i)$ for $\Psi_i = \sqrt{\rho_i}e^{i\theta_i}$. The quantity $\Omega(r)$ measures a density of pinned quantized vortices in the SF that may arise by the applied magnetic field. The momentum distribution is given as

$$n(\mathbf{k}) = \frac{1}{N}\sum_{i,j}\langle a_i^\dagger a_j\rangle e^{i\mathbf{k}\cdot(\mathbf{R}_i-\mathbf{R}_j)} = \frac{1}{N}\sum_{i,j}\Psi_i^*\Psi_j e^{i\mathbf{k}\cdot(\mathbf{R}_i-\mathbf{R}_j)}$$

in the Gutzwiller approximation. Quantity $n(\mathbf{k})$ clarifies the momentum $\mathbf{k}$ at which the BEC takes place. As the analytical study in Ref. [29] shows, a condensate with a nonvanishing $\mathbf{k}$ is expected to form. In the following numerical study, we shall verify the existence of such a condensation for certain parameter regions.

First, we consider the case of the vanishing NN repulsion $V = 0$, and show the numerical results. As we stated above, the magnetic flux per plaquette is $2\pi f = \pi$ and the density of the (excess) particle $\rho = 1.25$ ($\rho_{\rm ep} = 0.25$), i.e., the filling factor of the excess particle $\nu_{\rm ep} = \frac{0.25}{0.5} = \frac{1}{2}$.

The upper-left panel in Fig. 2 shows the phase diagram in the (J/U-μ/U) plane and also the line $\rho = 1.25$ is indicated. The cross symbol on the line $\rho = 1.25$ exhibits the parameter ($J/U = 0.05$, $\mu/U = 0.8$) on which we calculated the vortex density $\Omega(r)$ and the density momentum distribution $n(\mathbf{k})$. By the application of the magnetic field, the MI phase is elongated. The upper-middle panel shows that vortices are generated and they crystallize and form a solid pattern as a result of the pinning by the lattice and intervortex repulsion. In this vortex solid state, the momentum distribution $n(\mathbf{k})$ clearly exhibits a BEC at a finite momentum in the first magnetic Brillouin zone. The appearance of the same vortex solid pattern was shown for *deep SF states* by the previous work using large-scale Monte Carlo simulations [30]. The numerical results $\Omega(r)$ and $n(\mathbf{k})$ indicate that the BEC forms even though the condensation appears at nonvanishing $\mathbf{k}$ points. The state breaks the global U(1) symmetry of the phase rotation and, as a result, the ground state has a gapless excitation as we show later on. This state is the genuine SF.

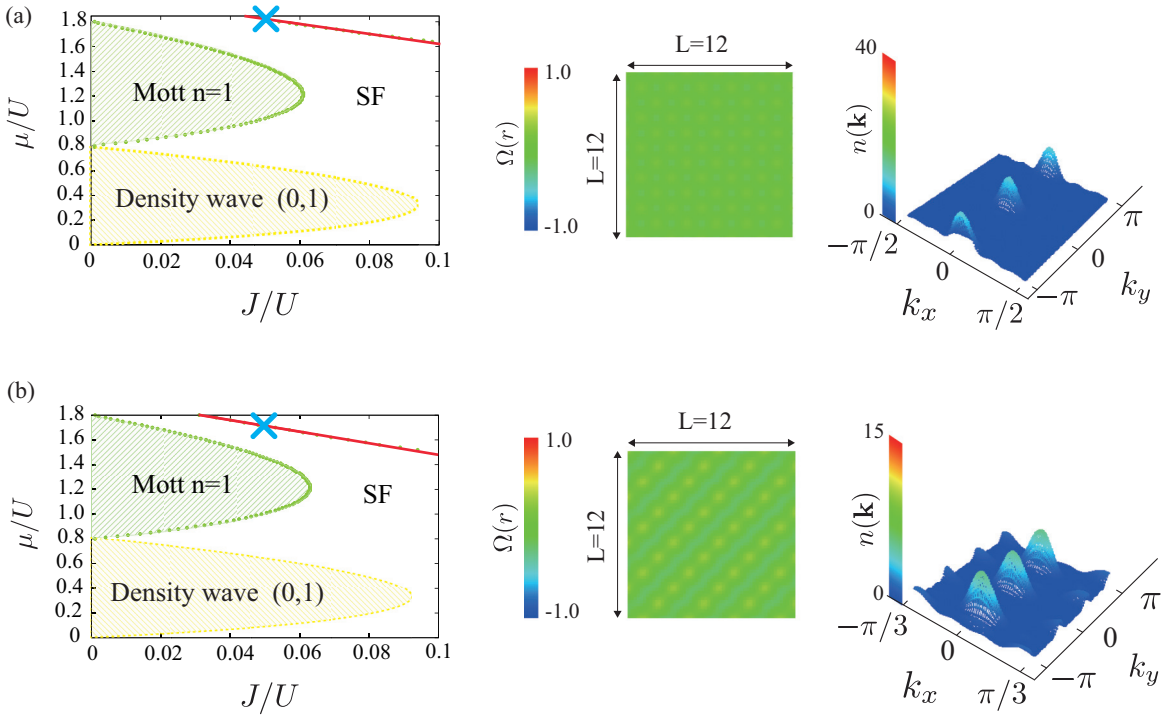

FIG. 3. Numerical results for the $V/U = 0.2$ and $J/U = 0.05$ cases. As in Fig. 2, the upper panels correspond to the $f = \frac{1}{2}$ case and the lower panels to the $f = \frac{1}{3}$ case. Calculations of $\Omega(r)$ and $n(\mathbf{k})$ are shown. In both cases, the signals of the vortex solid are weakened, in particular, in the $f = \frac{1}{2}$ case.

Similar results were obtained for the case $\nu_{\rm ep} = \frac{1}{2}$ with $f = \frac{1}{3}$ and $\rho = 1 + \frac{1}{6}$. See the lower panels in Fig. 2. The pattern of the vortex solid is the same with that observed in the previous work for the deep SF state with $f = \frac{1}{3}$ [30].

Let us study the effects of the NN repulsion. We studied the case $V/U = 0.2$, and the obtained phase diagrams are shown in Fig. 3. Finite NN repulsion shifts the MI-SF boundary and also the density-wave (DW) state with the density $\rho = \frac{1}{2}$ appears, in which the particle density at the even (odd) sublattice is unity (vanishing) or vice versa. We denote this state as (0,1) DW in Fig. 3. In order to study the case of the filling fraction $\nu_{\rm ep} = \frac{1}{2}$ near the MI with $\rho = 1$, we adjusted the chemical potential properly. The values of μ/U and J/U for the numerical study are indicated in the phase diagram in Fig. 3 by the cross symbol.

The calculated local vortex density $\Omega(r)$ and the momentum distribution $n(\mathbf{k})$ are shown in Fig. 3. Interestingly enough, the calculation of $\Omega(r)$ shows that the vortex solid melts, and a featureless state takes the place of the vortex solid. This result is confirmed by the calculation of $n(\mathbf{k})$. The result in Fig. 3 exhibits the smearing of peaks that existed in the case of $V = 0$. We also verified that there exists no phase coherence of Ψ_i, i.e., Ψ_i substantially changes spatially and also under the local update of $\{f_n^i\}$. From the above observation, we conclude that the obtained quantum state for $V/U = 0.2$ is *not* the SF, and the U(1) symmetry of the phase rotation is preserved. It is also obvious that the state under consideration is not the MI, and therefore it may be called "Bose metal."

In order to verify the above conclusion, we calculated the energy gap from the obtained ground states. In the single-mode approximation [31], the excitation spectrum in $\mathbf{k}$ space is given by

$$\Delta(\mathbf{k}) = \frac{\langle \Psi_{\rm GS}|\rho_{\mathbf{k}}^\dagger(\hat{H} - \epsilon_0)\rho_{\mathbf{k}}|\Psi_{\rm GS}\rangle}{\langle \Psi_{\rm GS}|\Psi_{\rm GS}\rangle}, \tag{3.6}$$

where $|\Psi_{\rm GS}\rangle$ denotes the ground-state wave function and ϵ_0 is its energy. The density operator $\rho_{\mathbf{k}}$ is given as follows in the second-quantized representation:

$$\rho_{\mathbf{k}} = \sum_\ell e^{i\mathbf{k}\cdot\mathbf{R}_\ell}\hat{n}_\ell, \quad \hat{n}_\ell = a_\ell^\dagger a_\ell.$$

By taking $\mathbf{k} \to \mathbf{0}$, $\Delta(\mathbf{0})$ gives an excitation gap from the ground state. We apply the above formulation to the Gutzwiller wave function, i.e., the ground-state wave function $|\Psi_{\rm GS}\rangle$ is taken to the Gutzwiller ground-state wave function $|\Psi_{\rm GW}\rangle$ obtained for the parameters from $V/U = 0$ to $V/U = 0.2$.

Figure 4 shows the excitation gaps of the ground states. The gap is vanishingly small for $0 < V/U < 0.1$ whereas it starts to increase as V/U increases from 0.1. This result indicates that the BEC realizes for small V but for $V/U > 0.1$, another gapped state appears as the above consideration suggests. Recently, similar gapped states have been reported in Ref. [18], where a cluster-type numerical mean-field method was used for the numerical calculation.

It is interesting to search another state that cannot be described by the site-factorized Gutzwiller wave function in Eq. (3.1). A candidate of such states is the bosonic FQH state. In Sec. V, we shall show that such a state can be described by the modified Gutzwiller wave function based on the idea of the flux attachment to particle and, in fact, it can be a candidate of the ground state with strong correlations. Before going into the details of the calculation, we review the lattice CS gauge theory for the bosons on the lattice in the following section.

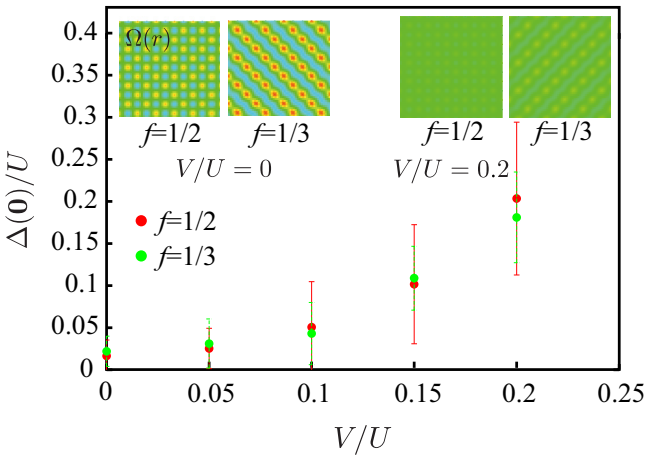

FIG. 4. Energy gaps calculated by the single-mode approximation for the states described by the Gutzwiller wave functions in the case $J/U = 0.05$. Applied magnetic field is $f = \frac{1}{2}$ and $\frac{1}{3}$ and $\rho \simeq 1.25$. As the NN repulsion V increases, the energy gap increases from the vanishing value. At $V = 0$, the stable vortex solid forms as the density profile in the inset indicates. As a result, the gapless Nambu-Goldstone boson exists. On the other hand for $V/U = 0.2$, the vortex solid melts and the SF is destroyed, and then the excitations acquire a gap. We took 50 samples in each measurement because the value of the excitation gap depends on initial values of $\{\Psi_i\}$.

IV. LATTICE CHERN-SIMONS THEORY FOR EXCESS PARTICLE AND EXCITATION GAP OF COMPOSITE BOSON

We apply the CS theory to the excess particle Hamiltonian (2.2). The CS theory succeeded in describing the FQH state in 2D electron system [8,9,20]. One of the authors previously introduced and formulated the lattice version of the CS theory for 2D lattice fermion system [32], and this formulation is well suited for study of the present boson system (see Fig. 5).

By using this formalism, we transform the original excess boson operator c_i in Eq. (2.2) to another particle operator b_i, which we call CS particle, by attaching $(\nu_{\rm ep})^{-1}$ magnetic flux quanta to c_i,

$$c_i = U_i b_i,$$
$$U_i = \exp\left[i\nu_{\rm ep}^{-1} \sum_{r'} \theta(i,r')(c_{i'}^\dagger c_{i'}) \right], \tag{4.1}$$

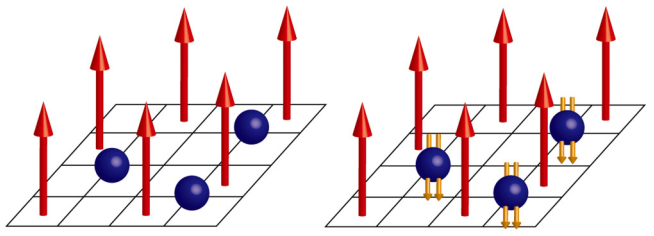

FIG. 5. Chern-Simons theory of lattice bosons in a strong magnetic field. Each boson is attached an even number of the flux quanta (orange arrow) of the CS gauge field. The external magnetic field (red arrow) is canceled out on the average by the CS gauge field.

where r (r') denotes a site of the dual lattice paired to site i (i') of the original lattice as before, and $\theta(i,r')$ is the azimuthal angle function on the lattice. As we consider the case in which $\nu_{\rm ep}^{-1}$ = an integer, the transformation (4.1) is well defined. Please notice $c_i^\dagger c_i = b_i^\dagger b_i$, and therefore

$$H_{\rm eBHM} = -J(n+1)\sum_{\langle i,j\rangle}(b_i^\dagger W_i^\dagger W_j b_j + \text{H.c.}) + \sum_i U(b_i^\dagger b_i - 1)b_i^\dagger b_i + V\sum_{\langle i,j\rangle} b_i^\dagger b_i b_j^\dagger b_j - \tilde{\mu}\sum_i b_i^\dagger b_i,$$
$$W_i = \exp\left[i\nu_{\rm ep}^{-1}\sum_{r'}\theta(i,r')(b_{i'}^\dagger b_{i'} - \rho_{\rm ep}) \right]. \tag{4.2}$$

Here, we have employed the symmetric gauge for $A_{i,\mu} \equiv A_{ij=i+\mu}$, and used the identity

$$2\pi\epsilon_{\mu\nu}\nabla_\nu G(r,r') = \nabla_\mu\theta(i,r'), \tag{4.3}$$

where $G(r,r')$ is the two-dimensional lattice Green function, i.e., $\sum_{\mu=1,2}\nabla_\mu^2 G(r,r') = -\delta_{rr'}$. The CS gauge theory can be constructed for the system in Eq. (4.2) in the Lagrangian formalism, but here we only discuss the possible mean-field solution of the ground-state and low-energy excitations of the above system. Hereafter as an example, we consider the mean excess particle density $\rho_{\rm ep} = \frac{1}{4}$ and the magnetic field $f = \frac{1}{2}$, and as a result $\nu_{\rm ep} = \frac{1}{2}$. The left panel in Fig. 2(a) indicates the line $\rho_{\rm ep} = \frac{1}{4}$. In the case $\nu_{\rm ep} = \frac{1}{2}$, two flux quanta are attached to one excess particle, and then the CS particle is bosonic, i,e., composite boson (CB). Also, we shall discuss a CF picture in Sec. VI.

If the CB forms a BEC in the system $H_{\rm eBHM}$ of Eq. (4.2), a bosonic analog of the FQH state is realized. In this case, the expectation value of the CB operator is the density $\rho_{\rm ep}$, which is uniform on the present lattice system as the external magnetic field is canceled by the CS gauge field at temperature $T = 0$, i.e., $\langle W_i\rangle = 1$. Under this assumption, we can calculate the energy gap from the Hamiltonian (4.2). We impose hard-core boson constraint, and then we drop the onsite interaction term with the coefficient U. This result comes from two reasons: excess particle density is dilute and we consider the large-U regime. We first set $V = 0$ for simplicity and the effect of the NN repulsion will be studied afterward.

We introduce a quantum fluctuation η_i from the condensation of the CB operator

$$b_i = \sqrt{\rho_{\rm ep}} + \eta_i. \tag{4.4}$$

The uniform density $\rho_{\rm ep}$ determines the chemical potential $\tilde{\mu}$. Substituting the uniform condensed variable $b_i \to b$, the Hamiltonian $H_{\rm eBHM}$ reduces to

$$H_{\rm eBHM} \to E_b = -4\tilde{J}|b|^2 - \tilde{\mu}|b|^2, \tag{4.5}$$

where we have put $\tilde{J} \equiv J(n+1)$. From this mean-field energy, the chemical potential is determined as

$$\frac{d}{db^*}E_b\Big|_{b=\sqrt{\rho_{\rm ep}}} = 0 \to \quad \tilde{\mu} = -4\tilde{J}. \tag{4.6}$$

From Eqs. (4.4) and (4.6), we derive the effective Hamiltonian of η_i. First, the hopping term in Eq. (4.2) is rewritten

as

$$\sum_{i,j}(b_i^\dagger W_i^\dagger W_j b_j + \text{H.c.}) = \sum_{i,\mu}(b_{i+\mu}^\dagger e^{i\delta A_{i,\mu}} b_i + \text{H.c.}), \tag{4.7}$$

where

$$\delta A_{i,\mu} = \frac{2\pi}{\nu_{\text{ep}}}\epsilon_{\mu\lambda}\sum_{i'}\nabla_\lambda G(r,r')[\sqrt{\rho_{\text{ep}}}(\eta_{i'}^\dagger + \eta_{i'}) + \eta_{i'}^\dagger\eta_{i'}]. \tag{4.8}$$

Substituting Eq. (4.4) into the Hamiltonian (4.2), and keeping terms up to the second order of the field η_i, we obtain the effective Hamiltonian with the quadratic order of η_i:

$$\begin{aligned} H_{\text{eBHM}} \to H_\eta = -\tilde{J}\sum_{i,\mu}[&-(\nabla_\mu\eta_i^\dagger)(\nabla_\mu\eta_i^\dagger) \\ &- i\sqrt{\rho_{\text{ep}}}\eta_i^\dagger(\nabla_\mu\delta A_{i,\mu}) + i\sqrt{\rho_{\text{ep}}}\eta_i(\nabla_\mu\delta A_{i,\mu}) \\ &- \rho_{\text{ep}}(\delta A_{i,\mu})^2], \end{aligned} \tag{4.9}$$

where we have neglected an irrelevant constant. By using the properties of the Green function

$$(\nabla_\mu)^2 G(r,r') = -\delta_{rr'} \text{ and } \epsilon_{\mu\lambda}\nabla_\mu\nabla_\lambda G(r,r') = 0,$$

we obtain the final form

$$\begin{aligned} H_\eta = &\sum_{i,\mu}\tilde{J}(\nabla_\mu\eta_i^\dagger)(\nabla_\mu\eta_i^\dagger) \\ &+ \sum_{i,i'}\tilde{J}(2\pi f)^2(\eta_i^\dagger + \eta_i)G(r,r')(\eta_{i'}^\dagger + \eta_{i'}). \end{aligned} \tag{4.10}$$

The second term of this Hamiltonian H_η is the contribution from the CS gauge field $\delta A_{i,\mu}$. As we show, this CS gauge coupling gives a finite mass to the "would-be massless Nambu-Goldstone boson" as a result of the long-range interactions [33,34].

We use the Fourier-transformed representation of H_η. The lattice Green function $G(r,r')$ is explicitly given as [35,36]

$$G(r,r') = \int \frac{d^2k}{(2\pi)^2}\frac{e^{ik(r-r')}}{4 - 2\sum_\mu \cos(k_\mu)}. \tag{4.11}$$

It should be noticed that this function has an infrared singularity but its derivative is well defined. Substituting Eq. (4.11) into (4.10) and then taking the Fourier transformation, we obtain the following Hamiltonian by using the Nambu representation $\vec{\eta} = (\eta(k), \eta^\dagger(-k))^t$:

$$\begin{aligned} H_\eta &= \int_{k>0}\frac{d^2k}{(2\pi)^2}\vec{\eta}^\dagger(k)\hat{H}_\eta\vec{\eta}(k), \\ \hat{H}_\eta &\equiv \begin{bmatrix} \epsilon(k) + 2\alpha & 2\alpha \\ 2\alpha & \epsilon(k) + 2\alpha \end{bmatrix}, \\ \epsilon(k) &\equiv \tilde{J}\left[4 - 2\sum_\mu \cos(k_\mu)\right], \quad \alpha = \frac{\tilde{J}(2\pi f)^2}{4 - 2\sum_\mu \cos(k_\mu)}. \end{aligned} \tag{4.12}$$

It is easy to carry out the Bogoliubov transformation for this matrix $\hat{H}_\eta$; we calculate the eigenvalues of the matrix $\sigma_3\hat{H}_\eta$ to obtain the excitation energy, where the σ_3 is the z component of the Pauli matrix [37]. This computation preserves the Bose commutation relation. Thus, the matrix is directly diagonalized by multiplying a unitary operator $\hat{\mathcal{U}}$ and the excitation energy is obtained as

$$\begin{aligned} \hat{\mathcal{U}}\sigma_3\hat{H}\hat{\mathcal{U}}^\dagger &= \begin{bmatrix} E(k) & 0 \\ 0 & E(-k) \end{bmatrix}, \\ E(k) &= \{[\epsilon(k) + 2\alpha]^2 - 4\alpha^2\}^{\frac{1}{2}}. \end{aligned} \tag{4.13}$$

By taking the long wave limit, we have

$$E(k) \xrightarrow{\mathbf{k}\to 0} 2(n+1)J(2\pi f) = 2(n+1)J\Phi, \tag{4.14}$$

where $\Phi = 2\pi f$ is the magnitude of the magnetic flux per plaquette. The above result indicates that the excitation energy of the excess CB is gapped. We plot the energy spectrum (4.13) in Fig. 6(a).

Here, we should remark that in the vicinity of Mott state there are two independent gapped excitations: the one comes from this CB boson sector and the other from the based Mott state. However, the former gap only depends on the parameter J as in Eq. (4.14). Therefore, the measurement of this energy gap seems feasible in recent experiments. This point will be discussed in Sec. VII.

Let us see the effect of the NN repulsion. It is not difficult to introduce the NN repulsion $V\sum_{i,j} n_i n_j$ in the above calculation. In particular for the case $U > V$, the calculation is rather straightforward. By using Eqs. (4.12) and (4.13), the chemical potential $\tilde{\mu}$ is estimated as $\tilde{\mu} = -4\tilde{J} + 4V\rho_{\text{ep}}$. Then, the quadratic terms of the fluctuation η_i come from the term

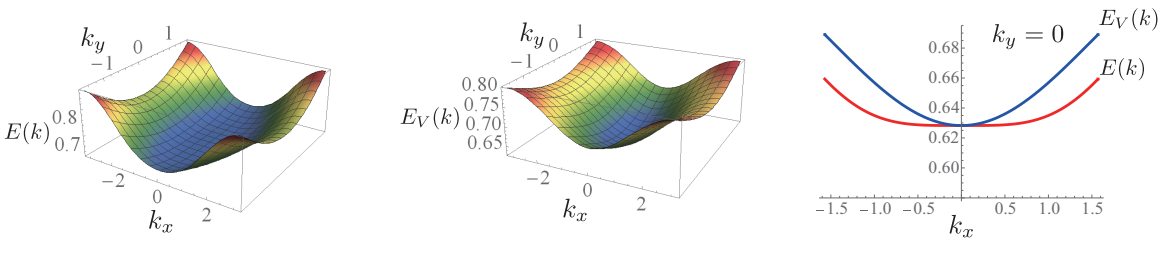

(a) (b) (c)

FIG. 6. Bogoliubov excitation spectrum of $\tilde{J}/U = 0.1$ (a) for $V/U = 0$ and (b) $V/U = 0.2$. (c) Dispersion relations for $V/U = 0$ and $V/U = 0.2$, $E(k)$ and $E_V(k)$, in the plane $k_y = 0$. $E(0) = E_V(0)$, however, $E_V(k) > E(0)$ for $\mathbf{k} \neq 0$. This indicates the stability of the CB picture for $V > 0$.

$V\sum_{i,j} n_i n_j$ are obtained as follows:

$$V\left[\sum_i (4\rho_{\rm ep}\eta_i^\dagger\eta_i) + \sum_{\langle i,j\rangle}\rho_{\rm ep}(\eta_i^\dagger+\eta_i)(\eta_j^\dagger+\eta_j)\right]. \quad (4.15)$$

Adding these terms to Eq. (4.10) and using the Bogoliubov transformation as before, we obtain the excitation spectrum including V term as

$$E_V(k) = \{[\epsilon(k) + 2\alpha + 2\rho_{\rm ep}V\gamma(k)]^2 - [2\alpha + 2\rho_{\rm ep}V\gamma(k)]^2\}^{\frac{1}{2}}, \quad (4.16)$$

where $\gamma(k) = \sum_{\mu=1,2}\cos(k_\mu)$. In Fig. 6(b), we plot $E_V(k)$. The value of the energy gaps $E(0)$ and $E_V(0)$ are the same, but as shown in Fig. 6(c), the curvature of $E_V(k)$ around $\mathbf{k} = \mathbf{0}$ is larger than that of $E(k)$. Therefore, we expect that the ground state of a finite NN repulsion system is more stable than that of $V = 0$ as excitations with a finite momentum are suppressed by the NN repulsion.

In Sec. V, based on the study of the CS theory in this section, we shall introduce a wave function of the CB. It has a form of the Gutzwiller type but contains strong correlations between bosons as described by the CS gauge theory. We calculate the ground-state energy of the states and compare it with that of the obtained states in Sec. III. Through the comparison, we can judge which state is a better candidate for the ground state.

V. CHERN-SIMONS GUTZWILLER APPROXIMATION OF EXCESS PARTICLE

In this section, we shall formulate the CS-Gutzwiller theory for the excess particle system whose Hamiltonian is given by Eq. (2.2). Wave function for the bosonic analog of the FQH state is constructed by using the singular gauge transformation similarly to Eq. (4.1) in Sec. IV. Then, we calculate the energy of the ground state and compare it with that of the state obtained by the simple Gutzwiller approximation in Sec. III. We consider both $V/U = 0$ and 0.2 cases. This formulation is nothing but the bosonic counterpart of the CB approach for the electron FQH state.

A. Chern-Simons transformation and the Gutzwllier approximation

In the CS theory for the CB, fictitious flux quanta are attached to particle. As a result, the CBs have strong correlation with each other through the Aharanov-Bohm effect. In the present case, the number of the attached flux quanta is $1/\nu_{\rm ep}$. In the mean-field approximation, the external magnetic field and the magnetic field of the fictitious gauge field (the CS gauge field) cancel out with each other, and the homogeneous BEC of the CB is a possible ground state of the system.

Let us recall the excess particle Hamiltonian $H_{\rm eBHM}$, and the Gutzwiller wave function $|\Psi_{\rm GW}\rangle$:

$$H_{\rm eBHM} = -J(n+1)\sum_i (c_{i+\mu}^\dagger e^{iA_{i,\mu}}c_i + {\rm H.c.}) + \sum_i U(n_i-1)n_i + V\sum_{\langle i,j\rangle} n_{c,i}n_{c,j} - \tilde{\mu}n_i, \quad |\Psi_{\rm GW}\rangle = \prod_{i=1}^N\left(\sum_{n=0}^{n_c} f_n^i|n\rangle_i\right).$$

The above wave function $|\Psi_{\rm GW}\rangle$ is site factorized and no correlation exists in particles at different sites. In order to attach the flux quanta to particles, we introduce the following unitary transformation $U_{\rm G}$:

$$U_G = \prod_{i=1}^N W_i, \quad (5.1)$$

$$W_i = e^{i\nu_{\rm ep}^{-1}\sum_{j\neq i}\theta(i,j)n_j}, \quad (5.2)$$

which is the first-quantization representation of the operator U_i in Eq. (4.1). This transformation U_G is nothing but the CS transformation on the lattice [38,39]. By applying the unitary transformation U_G to the simple Gutzwiller wave function $|\Psi_{\rm GW}\rangle$, the flux-attached wave function $|\Psi_{\rm CS}\rangle$, which we call CS wave function, is produced:

$$|\Psi_{\rm CS}\rangle = \prod_{i=1}^N W_i|\Psi_{\rm GW}\rangle = \prod_{i=1}^N\left(\sum_{n=0}^{n_c} W_i f_n^i|n\rangle_i\right) \equiv \prod_{i=1}^N\left(\sum_{n=0}^{n_c}\gamma_n^i|n\rangle_i\right), \quad (5.3)$$

$$\gamma_n^i \equiv e^{i\nu_{\rm ep}^{-1}\sum_{j\neq i}\theta(i,j)n_j} f_n^i. \quad (5.4)$$

As $\{\gamma_n^i\}$ in Eq. (5.4) show, $|\Psi_{\rm CS}\rangle$ represents a strongly correlated state (see Fig. 5). The state $|\Psi_{\rm CS}\rangle$ is a candidate for the ground state for specific fillings, and physical quantities like energy are calculated as

$$E_{\rm CS} = \langle\Psi_{\rm CS}|H_{\rm eBHM}|\Psi_{\rm CS}\rangle. \quad (5.5)$$

In the practical calculation, we employ the periodic boundary condition. The summation in Eq. (5.4) takes only once for each site $j \neq i$.

In the following subsection, we obtain the CS wave function of the ground state by the Gutzwllier method and calculate its energy.

B. Numerical results

We have two candidates for the ground state within the Gutzwllier method: one is $|\Psi_{\rm GW}\rangle$ and the other is $|\Psi_{\rm CS}\rangle$, which are defined by Eqs. (3.1) and (5.3), respectively. We calculated the energy of the two states by the Gutzwllier approximation. To see which state has a lower energy, we have to carefully define the energy of excess particles.

For the state $|\Psi_{\rm GW}\rangle$, the energy of the MI has to be subtracted. In the MI, the particle number at each site is unity with only very small fluctuations. Also, the local density terms including the chemical potential term $-(\frac{U}{2}+\mu)n_i$ should be subtracted from the total energy as they only contribute to control the average particle density. Therefore, we define the excess particle energy in the $|\Psi_{\rm GW}\rangle$,

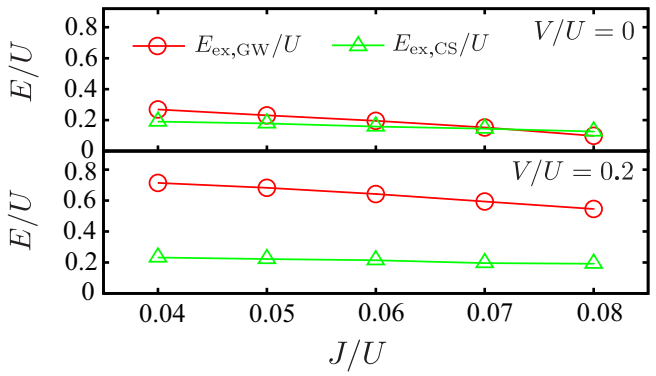

FIG. 7. Energies of the states described by the Gutzwiller wave function and the CS wave function, $E_{\mathrm{ex,GW}}$ and $E_{\mathrm{ex,CS}}$, respectively. For $V = 0$, these two states have comparable energy. On the other hand for $V/U = 0.2$, the CB state has a lower energy than the GW function state.

$E_{\mathrm{ex,GW}}$, as

$$E_{\mathrm{ex,GW}} \equiv \langle H_{\mathrm{BHM}} \rangle + (\mu + U/2)\sum_i \rho - \frac{U}{2}(1-1)1 - V\sum_{\langle i,j\rangle} 1 \times 1,$$

where $\rho = 1.25$ in the present case. On the other hand for the state $|\Psi_{\mathrm{CS}}\rangle$,

$$E_{\mathrm{ex,CS}} \equiv E_{\mathrm{CS}} + (\tilde{\mu} + U)\rho_{\mathrm{ep}}.$$

As we stated above, we consider the two cases $V/U = 0$ and 0.2. If the particle density were sufficiently large, the vortex-lattice states observed for $V = 0$ in the magnetic field $f = \frac{1}{2}$ and $\frac{1}{3}$ were expected to be the genuine ground state, i.e., the optical lattice plays a role of the vortex pinning and stabilizes the vortex solid. However, in the present system, the density of the excess particle is very low, and therefore it is interesting to compare the vortex-lattice state in Sec. III to the CS ground state. On the other hand for the case with $V/U = 0.2$, we expect that the CS state $|\Psi_{\mathrm{CS}}\rangle$ has a lower energy than $|\Psi_{\mathrm{GW}}\rangle$ as there exists no order in the state $|\Psi_{\mathrm{GW}}\rangle$.

The numerical result for $0.04 \leqslant J/U \leqslant 0.08$ is shown in Fig. 7. For the $V = 0$ case, we find that both energies $E_{\mathrm{ex,GW}}$ and $E_{\mathrm{ex,CS}}$ are very close, i.e., the vortex solid phase competes with the excess particle FQH state. On the other hand for the $V/U = 0.2$ case, the energy of the state $|\Psi_{\mathrm{CS}}\rangle$, $E_{\mathrm{ex,CS}}$, is lower than $E_{\mathrm{ex,GW}}$ of the Bose-metal phase. *This result indicates that the finite NN repulsion prefers the bosonic analogs of the FQH state.* This is one of the main conclusions of this paper.

VI. COMPOSITE FERMION PICTURE

In this section, we continue the analytical study on the excess particle BHM with a relatively large NN repulsion V. As we showed in Sec. IV, the non-SF phase numerically observed in Sec. III for $V/U = 0.2$ is not a true ground state, and instead of it, the strongly correlated state, which is described by the CS wave function, is a good candidate for the genuine ground state.

The above study is based on the CB picture described by the CS gauge theory coupled with bosons. In this section, we employ the CF picture, which is another possible theory describing the FQH state of the hard-core bosons. In fact, the exact diagonalization for the system with a small size exhibits a good overlap between the CF wave function and that of the excess particle BHM [13]. In this section, we shall explain how the CF picture appears from the effective Hamiltonian of the excess particle in Eq. (2.2). In the previous paper [32], we studied dynamics of electrons in the half-filled Landau level, and showed that the CF picture appears as a result of "the particle-flux separation," which is a similar phenomenon to the spin-charge separation in the strongly correlated systems like the high-T_c cuprates.

We introduce a *fermion* ψ_i that is defined as follows:

$$\psi_i = \tilde{W}_i c_i, \quad c_i = \tilde{W}_i^\dagger \psi_i,$$
$$\tilde{W}_i = \exp\left[ip\sum_{r'}\theta(i,r')c_{i'}^\dagger c_{i'}\right] = \exp\left[ip\sum_{r'}\theta(i,r')\psi_{i'}^\dagger \psi_{i'}\right], \tag{6.1}$$

where p is *an odd integer* that is determined shortly and the other notations are the same with those in Sec. IV. Then, it is not so difficult to show that ψ_i's satisfy the fermionic anticommutation relations, and the original boson is expressed as a composite of ψ_i and the p-flux quanta. One may think that the strong onsite repulsion generating the MI produces fermionic properties of the excess particles, but the onsite repulsion itself is not enough to generate the CF picture as we see in this section. The hopping term of the Hamiltonian, H_{J}, is expressed as follows in terms of ψ_i:

$$H_{\mathrm{J}} = -\tilde{J}\sum_{i,\mu}(\psi_i^\dagger \tilde{W}_i \tilde{W}_{i+\mu}^\dagger)e^{iA_{i,\mu}^{\mathrm{ex}}}\psi_{i+\mu} + \mathrm{H.c.}$$
$$= -\tilde{J}\sum_{i,\mu}(\psi_i^\dagger e^{-iA_{i,\mu}^{\mathrm{eff}}}\psi_{i+\mu}, + \mathrm{H.c.}), \tag{6.2}$$
$$A_{i,\mu}^{\mathrm{ex}} = \sum_{i'}\nabla_\mu\theta(i,r')f, \quad \mathrm{rot}\, A_{i,\mu}^{\mathrm{ex}} = 2\pi f,$$
$$A_{i,\mu}^{\mathrm{eff}} = \sum_{i'}\nabla_\mu\theta(i,r')[p\psi_{i'}^\dagger\psi_{i'} - f], \tag{6.3}$$

where we have used Eq. (4.3) and A^{ex} denotes the vector potential of the external magnetic field in the symmetric gauge. From Eq. (6.3), it is obvious that when the fermion ψ_i has a homogeneous distribution with the average density per site ρ_{ep} and also the parameters satisfy the relation $f = (p-1)\rho_{\mathrm{ep}}$, we have $\langle \mathrm{rot}\, A_{i,\mu}^{\mathrm{eff}}\rangle = 2\pi\rho_{\mathrm{ep}}$. Therefore, *the fermions ψ_i fill just the Hofstadter bands ramifying from the lowest Landau level if interactions between ψ_i are irrelevant*. However, the fermion ψ_i has a nonlocal interaction with each other through $A_{i,\mu}^{\mathrm{eff}}$ in Eq. (6.3), and therefore an elaborate discussion is needed to justify the above assumption.

To study the above strongly correlated fermion system, we introduce the following slave-particle representation:

$$\psi_i = \phi_i \zeta_i, \tag{6.4}$$

where ϕ_i is a hard-core boson and ζ_i is a fermion, and we call ζ_i and ϕ_i chargon and fluxon, respectively. It is not so difficult to show that ψ_i's in Eq. (6.4) satisfy the fermionic anticommutation relation. The physical state condition of the slave-particle Hilbert space is given by the local constraint

$$\zeta_i^\dagger \zeta_i = \phi_i^\dagger \phi_i. \tag{6.5}$$

By the local constraint (6.5), we can prove

$$\psi_i^\dagger \psi_i = \zeta_i^\dagger \zeta_i \phi_i^\dagger \phi_i = \zeta_i^\dagger \zeta_i \zeta_i^\dagger \zeta_i = \zeta_i^\dagger \zeta_i = \phi_i^\dagger \phi_i. \tag{6.6}$$

Then, the nonlocal operator $\tilde{W}_i$ in Eq. (6.1) is expressed as

$$\tilde{W}_i = \exp\left[ip \sum_{r'} \theta(i,r') \phi_{i'}^\dagger \phi_{i'} \right] \equiv W_i^\phi. \tag{6.7}$$

The Hamiltonian $H_{\rm eBHM}$ is expressed as follows in the slave-particle representation:

$$\begin{aligned} H_{\zeta\phi} = & -J \sum \left(\zeta_{i+\mu}^\dagger \phi_{i+\mu}^\dagger W_{i+\mu}^\phi W_i^{\phi\dagger} e^{iA^{\rm ex}} \phi_i \zeta_i + {\rm H.c.} \right) \\ & - L_{\rm int} - \sum (\mu_\zeta \zeta_i^\dagger \zeta_i + \mu_\phi \phi_i^\dagger \phi_i) \\ & - \sum \lambda_i (\zeta_i^\dagger \zeta_i - \phi_i^\dagger \phi_i), \end{aligned} \tag{6.8}$$

where λ_i is the Lagrange multiplier for the local constraint (6.5), and $L_{\rm int}$ denotes the NN repulsion in $H_{\rm eBHM}$ in Eq. (2.2).

In order to study the above fermion system, we employ a Lagrangian formalism with an imaginary time τ. The partition function Z and the Lagrangian $L_{\zeta\phi}$ are given as follows:

$$\begin{aligned} Z &= \int [d\zeta][d\phi] \exp\left(\int_0^\beta d\tau \, L_{\zeta\phi} \right), \\ L_{\zeta\phi} &= -\sum \zeta_x^\dagger \partial_\tau \zeta_x - \sum \phi_x^\dagger \partial_\tau \phi_x - H_{\zeta\phi}, \end{aligned} \tag{6.9}$$

where x denotes the three-dimensional (3D) coordinate $x = (\tau, i)$ ($\tau \in [0,\beta]$), and $\beta = 1/(k_B T)$ with the Boltzmann constant k_B and temperature T. Then, we apply the following Hubbard-Stratonovich transformation to the above system $L_{\zeta\phi}$:

$$Z = \int [d\zeta][d\phi][dV] \exp\left(\int_0^\beta d\tau \, L_{\zeta\phi V} \right), \tag{6.10}$$

where

$$\begin{aligned} L_{\zeta\phi V} = & -\sum \zeta_x^\dagger (\partial_\tau + i\lambda_x - \mu_\zeta) \zeta_x - \sum \phi_x^\dagger (\partial_\tau - i\lambda_x - \mu_\phi) \phi_x \\ & + J \sum [V_{x\mu} (\phi_{x+\mu} W'_{x+\mu} W'^\dagger_x \phi_x^\dagger + \zeta_{x+\mu}^\dagger e^{ia_\mu} \zeta_x) + {\rm H.c.}] \\ & + J \sum (\phi_{x+\mu}^\dagger \phi_{x+\mu} \phi_x^\dagger \phi_x + \zeta_{x+\mu}^\dagger \zeta_{x+\mu} \zeta_x^\dagger \zeta_x) \\ & - J \sum |V_{i\mu}|^2 + L_{\rm int} \end{aligned} \tag{6.11}$$

and

$$\begin{aligned} W'_x &= W_x^\phi e^{-ip \sum_{r'} \theta(x,r') \rho_{\rm ep}} \\ &= \exp\left[ip \sum_{r'} \theta(x,r') (\phi_{x'}^\dagger \phi_{x'} - \rho_{\rm ep}) \right], \\ a_\mu &= \sum_{r'} \nabla_\mu \theta(x,r') (p\rho_{\rm ep} - f). \end{aligned} \tag{6.12}$$

Several comments on the system $L_{\zeta\phi V}$ in Eq. (6.11) are in order:

(1) The fields λ_i and $V_{i\mu}$ behave like a gauge field. In fact, *$L_{\zeta\phi V}$ is invariant under a time-dependent local gauge transformation*

$$(\zeta_i, \phi_i, V_{i\mu}, \lambda_i) \to (e^{i\alpha_i} \zeta_i, e^{-i\alpha_i} \phi_i, e^{i\nabla_\mu \alpha_i} V_{i\mu}, \lambda_i - \partial_\tau \alpha_i).$$

(2) Low-energy properties of the system are determined by the dynamics of the gauge field $V_{i\mu}$. If its dynamic is realized in a deconfinement phase like the Coulomb phase, the fields ζ_i and ϕ_i, chargon and fluxon, describe quasiexcitations, whereas in the confinement phase, the original boson is the only physically observable object. We call the phenomenon in the former case *particle-flux separation*.

(3) There appears the NN attractive force in the channel $(\zeta_{i+\mu} - \zeta_i)$ and $(\phi_{i+\mu} - \phi_i)$. This attractive force makes the system unstable into a phase separated state if the particle-flux separation takes place. In order to make the system stable, *the existence of the NN repulsion $L_{\rm int}$ is needed*.

(4) In the particle-flux separated state, the fluxon ϕ is nothing but a fermion in the commensurate external magnetic field. This fermion is defined as $\varphi_i = W_i^\phi \phi_i$ and φ_i feels the effective magnetic field $f_\varphi = p\rho_{\rm ep}$. As the density of φ_i is $\rho_{\rm ep}$, φ_i fills the $1/p$ levels in the lowest Hofstadter bands ramifying from the lowest Landau level in the continuum.

(5) a_μ is the vector potential that represents the magnetic field with flux quanta $(f - p\rho_{\rm ep}) = (f - f_\varphi)$ per plaquette. Then, it is obvious that η_i is nothing but the CF if the particle-flux separation is realized. The Hofstadter butterfly [24] predicts the parameters $(\rho_{\rm ep}, f)$ at which gapful states appear.

The above gauge-theoretical consideration gives a basis of the CF picture proposed by Möller and Cooper for the low-filling bosons on the lattice [13]. In their work, $p = 1$ and the trial CF-state wave function is given as (in their notation)

$$\Psi_{\rm trial}(\{\vec{r}_i\}) = \Psi_{\rm J}(\{\vec{r}_i\}) \times \Psi_{\rm CF}(\{\vec{r}_i\}), \tag{6.13}$$

where both of $\Psi_{\rm J}$ and $\Psi_{\rm CF}$ are fermionic wave functions. $\Psi_{\rm J}$ comes from the flux attachment and $\Psi_{\rm CF}$ is the wave function of the CF. In our derivation, *$\Psi_{\rm J}$ is nothing but the wave function of φ_i and $\Psi_{\rm CF}$ is that of ζ_i. Our study in this section has clarified the condition that the CF picture appears as quasiexcitations at low energy*. The problem of the gauge dynamics of the system $L_{\zeta\phi V}$ can be studied by the hopping expansion and the realization of the deconfinement phase (Coulomb-type phase) is suggested at low temperature [40]. However, a more detailed study is needed to reach a decisive conclusion. This problem is under study and the results will be published in the near future.

There is an ambiguity in the way of decoupling the hopping term in $H_{\zeta\phi}$ in Eq. (6.8) by the auxiliary field $V_{i\mu}$. We call the decoupling in Eq. (6.11) *optimal particle-flux separation*. In fact in $L_{\zeta\phi V}$ in Eq. (6.11), the chargon and fluxon do not interact with each other except the gauge interaction through $V_{i\mu}$. In the previous paper, we studied the *half-filled Landau level state* of 2D electron systems in a strong magnetic field. There, we used another decoupling in which the chargon feels magnetic fluxes carried by the fluxon. As a result of a BEC of the fluxon, the external magnetic field is totally shielded and

the CF behaves like a gapless fermion with a Fermi line in the momentum space. For this case, it is known that the dynamics of the gauge field $V_{i\mu}$ realizes a deconfinement phase and therefore the CF picture is justified [40].

At present, relationship between the CB and CF approaches is not clear. We shall study this problem in detail and hope that experiments on the cold atomic gases give an important clue to solve this problem.

VII. DISCUSSION AND CONCLUSION

In this paper, we have studied the ground-state properties of lattice bosons in the strong magnetic field in the vicinity of the Mott states. We have first rederived the excess particle effective Hamiltonian from the BHM with the NN repulsions. By using the Gutzwiller numerical method, we obtained the phase diagrams and investigated the ground-state properties for particular points near the Mott lobes for which the appearance of the bosonic analogs of the FQH state is expected. We have found that the vortex solids form in the absence of the NN repulsion, but a finite NN repulsion destabilizes the vortex solids and the featureless homogeneous state appears as the ground state of the Gutzwiller wave function that we call the Bose metal.

In order to investigate the ground state in the system with finite NN repulsions in detail, we have made use of the CS theory for the excess particle system. After the analytical study of the CS theory for the lattice boson in the strong magnetic field, we have applied the CS theory to the Gutzwiller numerical method and proposed the CS wave function for describing the bosonic FQH state. Then, we calculated the ground-state energies of the state given by the Gutzwiller wave function and the state of the CS wave function. We found that the NN repulsions prefer the state of the CS wave function.

We expect that the measurement of the energy gaps calculated in Secs. III, IV, and VI is feasible in real experiments on ultracold atomic gases. As one example, the lattice modulation method inducing the two-photon Bragg spectroscopy [41,42] may be efficient. If the bosonic FQH state or the Bose metal forms in real experiments, the total system has two energy gaps, i.e., one is the particle-hole excitation gap U in the base Mott state and the other is the excitation gap of the excess particle. On the other hand, if the system forms the vortex solid, i.e., the superfluid of the finite-momentum mode BEC, there exists a gapless excitation as a result of the spontaneous breaking of the U(1) symmetry.

Finally, we have studied the CF theory for the excess particle by using the CS theory. Our previous gauge-theoretical study on the electron system of the half-filled Landau level [32] is applicable rather straightforwardly to the present boson systems, and we showed the condition that the CF appears as quasiexcitations at low temperature.

We shall study the BHM with the NN repulsions by means of the exact diagonalization, the cluster Gutwiller method, etc., and examine the obtained results in this paper. In particular at present, the relationship between the CB and CF approaches to the 2D strongly correlated systems in a strong magnetic field is not understood. We expect that the ultracold atomic system plays an important role to solve this problem because of its controllability and versatility. We shall study this problem by means of the analytical and numerical methods mentioned above and propose experimental setups for testing the CB and CF pictures.

ACKNOWLEDGMENTS

Y.K. acknowledges the financial support of a Grant-in-Aid for JSPS Fellows (Grant No. 15J07370). This work was partially supported by JSPS KAKENHI Grant No. JP26400246.

APPENDIX: ESTIMATION OF PARAMETERS OF BHM FOR REAL EXPERIMENTS

In this Appendix, we microscopically evaluate the onsite and nearest-neighbor (NN) interactions (i.e., U and V) in the BHM of Eq. (2.1) as the ratio V/U plays an important role in this work for experimental realization. We assume the ratio $V/U \sim 0.2$, and therefore it is needed that the NN interaction V is comparable with the onsite interaction U. As we show, in real experiment, such a condition is feasible by using large magnetic dipolar atoms such as Cr, Er, and Dy [19]. In fact, by using dipolar atoms and the Feshbach resonance techniques, one can control the ratio V/U rather freely. Generally in a dipolar atom system, the onsite U is given as $U = U_s + U_d$, where U_s is the contribution from the s-wave scattering and U_d is the contribution from the dipole-dipole interaction. Also, the dipole-dipole interaction gives the NN interaction in the lattice system. In the case that the dipoles of atoms are perpendicular to the two-dimensional plane, the NN interaction is given as follows:

$$V = \int d\mathbf{r}\, d\mathbf{r}' |w_i(\mathbf{r})|^2 \left[\frac{\mu_0 \mu^2 G_{\mathbf{r}-\mathbf{r}'}}{4\pi |\mathbf{r}-\mathbf{r}'|^3}\right] |w_j(\mathbf{r}')|^2, \tag{A1}$$

$$G_{\mathbf{r}-\mathbf{r}'} = 1 - 3\cos^2\theta_{\mathbf{r}-\mathbf{r}'}, \tag{A2}$$

where μ_0 and μ are the permeability of vacuum and magnetic permeability of the dipolar atom, respectively, and $\theta_{\mathbf{r}-\mathbf{r}'}$ is the angle between $(\mathbf{r}-\mathbf{r}')$ and the orientation of the dipole. $w_{i(j)}(\mathbf{r})$ is the lowest-band Wannier function, which is tightly localized at site $i(j)$. As the above overlap integral (A1) shows, the value V is determined by the choice of dipolar atom.

In order to increase the ratio $V/U = V/(U_s + U_d)$, it is necessary to reduce the value of $U_s + U_d$. This is feasible in real experiments by controlling the parameter U_s, i.e., by controlling the s-wave scattering length a_s by the Feshbach resonance techniques [1,43]. Even if the value U_d has a large positive value compared to V, the small or negative value of U_s can reduce the total value of $U_s + U_d$. As we show, U_d has a strong dependence on the optical lattice potential and it can have even a negative value.

For future experiments, we shall estimate the BHM parameters J, U, and V. In particular, we estimate the value of tunable s-wave scattering length a_s for $V/U = 0.2$ and 0.3 to be realized.

Then, we consider a two-dimensional lattice similar to the recent experimental setup [44], and ^{168}Er for the dipolar atom with the moment $\mu = 7\mu_B$ (μ_B is Bohr magneton). We consider two-dimensional optical lattice potential with the lattice spacing $d = 266$ nm. This potential is explicitly

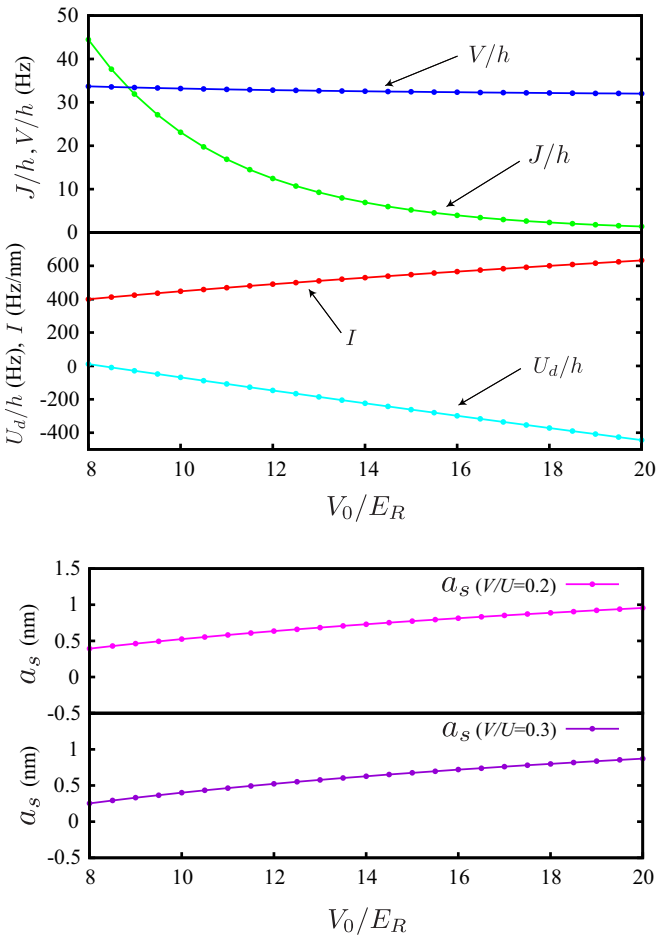

FIG. 8. Parameters of BHM evaluated microscopically as a function of V_0/E_R and the s-wave scattering length a_s for the experimental setup. The value of a_s is obtained as $a_s(V_0) = [V/\alpha - U_d]/I$, where $\alpha = V/U = 0.2$ or 0.3.

given as

$$V(\mathbf{r}) = V_0\{\cos^2[(2\pi/\lambda)x] + \cos^2[(2\pi/\lambda)y]\} + \tfrac{1}{2}m\omega_z^2 z^2, \tag{A3}$$

where V_0 is the potential depth and λ is the laser wavelength, m is the atom mass, and ω_z is the frequency of the harmonic trap used to construct the quasi-two-dimensional system. Here, the optical lattice spacing is given as $d = \lambda/2$. In this system, the other BHM parameters are given by the overlap integrals similar to Eq. (A1) [44]:

$$J = -\int d\mathbf{r}\, w_i^*(\mathbf{r})\left[-\frac{\hbar^2\nabla^2}{2m} + V(\mathbf{r})\right] w_j(\mathbf{r}), \tag{A4}$$

$$U_s = \frac{4\pi\hbar^2 a_s}{m}\int d\mathbf{r}|w_i(\mathbf{r})|^4 \equiv a_s I, \tag{A5}$$

$$U_{\rm d} = \int d\mathbf{r}\, d\mathbf{r}'|w_i(\mathbf{r})|^2\left[\frac{49\mu_0\mu_B^2}{4\pi|\mathbf{r}-\mathbf{r}'|^3}G_{\mathbf{r}-\mathbf{r}'}\right]|w_i(\mathbf{r}')|^2, \tag{A6}$$

where $m = 2.78\times10^{-25}$ kg is the ^{168}Er atom mass. To estimate the above integrals, we employ the harmonic oscillator approximation for the optical lattice potential $V(\mathbf{r})$. In this approximation, the Wannier function $w_i(\mathbf{r})$ is replaced by the harmonic-oscillator wave function of the lowest energy

$$w_i(\mathbf{r}) = \sqrt{\frac{\beta}{\pi}}e^{-\frac{\beta}{2}[(x-x_i)^2+(y-y_i)^2]}\left[\frac{\beta_z}{\pi}\right]^{1/4}e^{-\frac{\beta_z}{2}(z-z_i)^2}, \tag{A7}$$

where $\beta \equiv \frac{2m}{\hbar^2}\sqrt{E_{\rm R}V_0}$ [$E_{\rm R}$ is the recoil energy $\equiv h^2/(2m\lambda^2) \sim h\times 4.2$ kHz for ^{168}Er], $\beta_z \equiv \frac{m\omega_z}{\hbar}$, and the spatial coordinate (x_i, y_i, z_i) is the three-dimensional coordinate of optical lattice site i. We take $\omega_z \sim 160$ kHz to confine atoms tightly in the two-dimensional plane [45].

We numerically calculated the above integrals (A1) and (A4)–(A6), and estimated the value a_s for the ratio $V/U = 0.2$ and 0.3. We verified that our estimation of the parameters is in good agreement with the previous works [45]. Figure 8 shows the calculated results of the values of J, V, I, and U_d as a function of the potential depth V_0. U_d is negative as $V_0/E_{\rm R}$ is getting large as mentioned above. The values of a_s for realizing the ration $V/U = 0.2$ and 0.3 are also shown there. From the results, to achieve $J/U = 0.05$ and the target ratio V/U, we found that for $V/U = 0.2$, $a_s \sim 0.70$ nm and $V_0 \sim 13.5E_{\rm R}$, and for $V/U = 0.3$, $a_s \sim 0.67$ nm and $V_0 \sim 15.0E_{\rm R}$. These values of a_s and V_0 are feasible for real experiments.

[1] I. Bloch, J. Dalibard, and W. Zwerger, Rev. Mod. Phys. **80**, 885 (2008).
[2] M. Lewenstein, A. Sanpera, and V. Ahufinger, *Ultracold Atoms in Optical Lattices: Simulating Quantum Many-body Systems* (Oxford University Press, Oxford, 2012).
[3] M. Aidelsburger, M. Atala, M. Lohse, J. T. Barreiro, B. Paredes, and I. Bloch, Phys. Rev. Lett. **111**, 185301 (2013).
[4] H. Miyake, G. A. Siviloglou, C. J. Kennedy, W. C. Burton, and W. Ketterle, Phys. Rev. Lett. **111**, 185302 (2013).
[5] D. Jaksch and P. Zoller, New J. Phys. **5**, 56 (2003).
[6] S. Tung, V. Schweikhard, and E. A. Cornell, Phys. Rev. Lett. **97**, 240402 (2006).
[7] R. A. Williams, S. Al-Assam, and C. J. Foot, Phys. Rev. Lett. **104**, 050404 (2010).
[8] Z. F. Ezawa, *Quantum Hall Effects: Field Theorectical Approach and Related Topics*, 2nd ed. (World Scientific, Singapore, 2008).
[9] S.-C. Zhang, Int. J. Mod. Phys. B **06**, 25 (1992).
[10] R. N. Palmer and D. Jaksch, Phys. Rev. Lett. **96**, 180407 (2006).
[11] A. S. Sørensen, E. Demler, and M. D. Lukin, Phys. Rev. Lett. **94**, 086803 (2005).
[12] M. Hafezi, A. S. Sørensen, E. Demler, and M. D. Lukin, Phys. Rev. A **76**, 023613 (2007).
[13] G. Möller and N. R. Cooper, Phys. Rev. Lett. **103**, 105303 (2009).
[14] L. Hormozi, G. Moller, and S. H. Simon, Phys. Rev. Lett. **108**, 256809 (2012).
[15] M. Ö. Oktel, M. Niţă, and B. Tanatar, Phys. Rev. B **75**, 045133 (2007).

[16] R. O. Umucalılar and E. J. Mueller, Phys. Rev. A **81**, 053628 (2010).
[17] R. O. Umucalilar and M. Ö. Oktel, Phys. Rev. A **76**, 055601 (2007).
[18] S. S. Natu, E. J. Mueller, and S. Das Sarma, Phys. Rev. A **93**, 063610 (2016).
[19] T. Lahaye, C. Menotti, L. Santos, M. Lewenstein, and T. Pfau, Rep. Prog. Phys. **72**, 126401 (2009).
[20] D. Tong, Lectures on the Quantum Hall Effect, arXiv:1606.06687.
[21] D. Jaksch, V. Venturi, J. I. Cirac, C. J. Williams, and P. Zoller, Phys. Rev. Lett. **89**, 040402 (2002).
[22] J. Zakrzewski, Phys. Rev. A **71**, 043601 (2005).
[23] D. van Oosten, P. van der Straten, and H. T. C. Stoof, Phys. Rev. A **63**, 053601 (2001).
[24] D. R. Hofstadter, Phys. Rev. B **14**, 2239 (1976).
[25] K. Sengupta and N. Dupuis, Phys. Rev. A **71**, 033629 (2005).
[26] M. Jreissaty, J. Carrasquilla, F. A. Wolf, and M. Rigol, Phys. Rev. A **84**, 043610 (2011).
[27] This concern also appears in solving the Gross-Pitaevskii (GP) equation. In the GP community, to avoid this concern an extended method was invented: the truncated-Wigner approximation [28].
[28] A. Sinatra, C. Lobo, and Y. Castin, J. Phys. B: At., Mol. Opt. Phys. **35**, 3599 (2002); P. B. Blakie, A. S. Bradley, M. J. Davis, R. J. Ballagh, and C. W. Gardiner, Adv. Phys. **57**, 363 (2008).
[29] S. Sinha and K. Sengupta, Europhys. Lett. **93**, 30005 (2011).
[30] Y. Kuno, T. Nakafuji, and I. Ichinose, Phys. Rev. A **92**, 063630 (2015).
[31] R. P. Feynman and M. Cohen, Phys. Rev. **102**, 1189 (1956).
[32] I. Ichinose and T. Matsui, Nucl. Phys. B **468**, 487 (1996); **483**, 681 (1997).
[33] Z. F. Ezawa, M. Hotta, and A. Iwazaki, Phys. Rev. B **46**, 7765 (1992).
[34] I. Ichinose, T. Matsui, and M. Onoda, Phys. Rev. B **52**, 10547 (1995).
[35] J. B. Kogut, Rev. Mod. Phys. **51**, 659 (1979).
[36] R. Savit, Rev. Mod. Phys. **52**, 453 (1980).
[37] A. Altland and B. Simons, *Condensed Matter Field Theory* (Cambridge University Press, Cambridge, 2006).
[38] J. K. Jain, Phys. Rev. Lett. **63**, 199 (1989).
[39] E. Fradkin, Phys. Rev. Lett. **63**, 322 (1989); A. Lopez and E. Fradkin, Phys. Rev. B **44**, 5246 (1991).
[40] See, for example, I. Ichinose, T. Matsui, and M. Onoda, Phys. Rev. B **64**, 104516 (2001).
[41] T. Stoferle, H. Moritz, C. Schori, M. Kohl, and T. Esslinger, Phys. Rev. Lett. **92**, 130403 (2004).
[42] M. Endres, T. Fukuhara, D. Pekker, M. Cheneau, P. Schauss, C. Gross, E. Demler, S. Kuhr, and I. Bloch, Nature (London) **487**, 454 (2012).
[43] S. Inouye, M. R. Andrews, J. Stenger, H.-J. Miesner, D. M. Stamper-Kurn, and W. Ketterle, Nature (London) **392**, 151 (1998).
[44] S. Baier, M. J. Mark, D. Petter, K. Aikawa, L. Chomaz, Z. Cai, M. Baranov, P. Zoller, and F. Ferlaino, Science **352**, 201 (2016).
[45] O. Dutta, M. Gajda, P. Hauke, M. Lewenstein, D.-S. Luhmann, B. A. Malomed, T. Sowinski, and J. Zakrzewski, Rep. Prog. Phys. **78**, 066001 (2015).